Fully Transparent and Distortion-Free Monotonically Stretchable Substrate by Nanostructure Alignment

Jung Hur, Hwaeun Park, Hyeongsu Oh, Sujin Jeong, Jinhan Cho, Jonghwi Lee, Seungjun Chung, Yongtaek Hong,* and Jeong Gon Son*

Stretchable devices, garnering increasing attention as next-generation form factors, have a crucial problem in that vertical contraction occurs during stretching, causing image distortion of stretchable displays and discomfort in skin-attached devices. Previous structural strategies to mitigate vertical contraction, such as auxetic reentrants and wrinkles, suffer from the drawback that their structure becomes visible during stretching. In this study, this issue is addressed by unidirectionally aligning nanoscopic cylinders within block copolymer elastomer films. Employing a shear-rolling process at high temperatures on thick films of polystyrene-*block*-polyisobutylene-*block*-polystyrene thermoplastic elastomers, macroscopic mechanical anisotropy is achieved, resulting in completely transparent and monotonically stretchable substrates devoid of vertical or depth distortion during deformation. Significantly, the unidirectional orientation of high-modulus cylindrical nanostructures induces macroscopic mechanical anisotropy with a modulus ratio exceeding five times. While the Poisson's ratio of conventional elastic materials hovers around ≈0.5, this mechanical anisotropy minimizes vertical contraction, yielding a Poisson's ratio below 0.07. Moreover, owing to the negligible size of the nanocylinders compared to visible-light wavelengths, the substrate can be monotonically uniaxially stretched while maintaining high transmittance without introducing distortions, surface undulations, or haziness, resulting in distortion-free stretchable substrates.

1. Introduction

Stretchable devices, which can operate under physical deformation without damaging the device,[1,2] have greater freedom of shape and movement, leading to potential applications in wearable devices,[3] health monitoring devices,[4,5] soft robotics,[6] and even in stretchable and dynamically moving displays.[7] However, stretchable materials inherently contract in the vertical direction when stretched in one direction to minimize volume change, which can lead to undesirable deformation and thus, as shown in **Figure 1a**, in a stretchable display, the vertical shrinkage causes individual pixels to rotate toward the center and draw closer together, resulting in curved edges and an inhomogeneous distribution of deformation across the whole area. Moreover, for devices attached to the skin, if the Poisson's ratio does not match that of the skin, unwanted deformation may cause discomfort to the skin.[8] This vertical contraction can be quantified by the Poisson's ratio, defined as the ratio between transverse strain (ϵ_t) and longitudinal strain (ϵ_l) stretched in

J. Hur, H. Oh, J. Cho, J. G. Son
Soft Hybrid Materials Research Center
Korea Institute of Science and Technology
Seoul 02792, Republic of Korea
E-mail: jgson@kist.re.kr
J. Hur, H. Oh, J. Cho, J. G. Son
KU-KIST Graduate School of Converging Science and Technology
Korea University
Seoul 02841, Republic of Korea

H. Park, S. Jeong, Y. Hong
Department of Electrical and Computer Engineering
Seoul National University
Seoul 08826, Republic of Korea
E-mail: yongtaek@snu.ac.kr
H. Park, S. Jeong, Y. Hong
Inter University Semiconductor Research Center (ISRC)
Seoul National University
Seoul 08826, Republic of Korea
J. Cho
Department of Chemical & Biological Engineering
Korea University
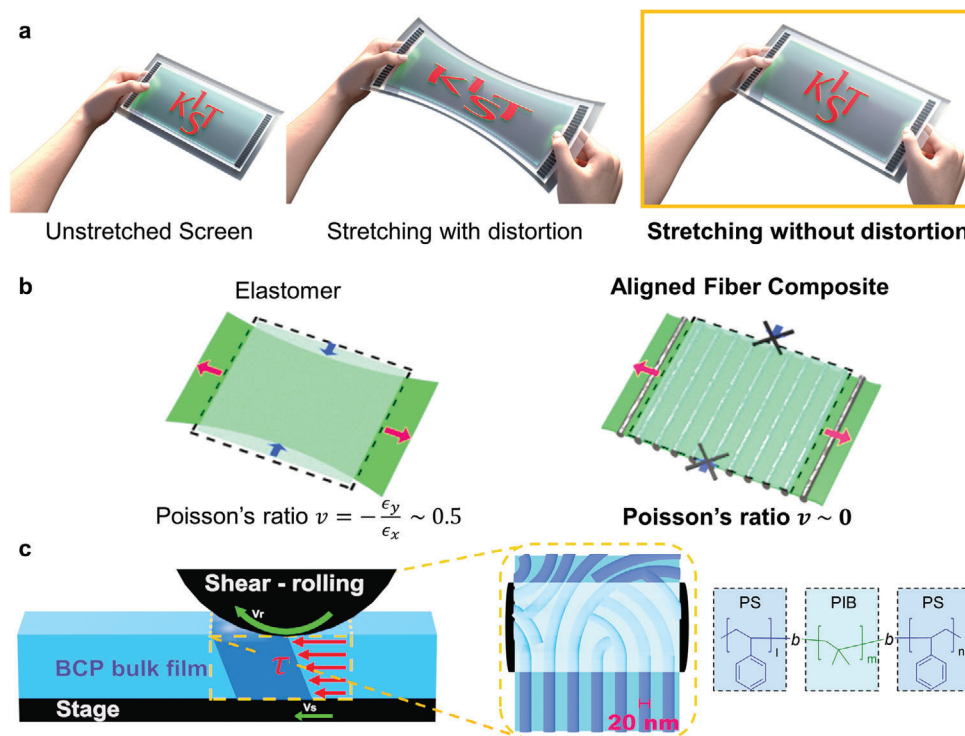Seoul 02841, Republic of Korea
J. Lee
School of Chemical Engineering and Materials Science
Chung-Ang University
Seoul 06974, Republic of Korea
S. Chung
School of Electrical Engineering
Korea University
Seongbuk-gu, Seoul 02841, Republic of Korea

**ADVANCED
SCIENCE NEWS**

www.advancedsciencenews.com

**ADVANCED
MATERIALS**

www.advmat.de

Figure 1. Unidirectionally aligned nanocylinders in block copolymer elastomers with mechanical anisotropy for realizing distortion-free stretchable substrate with full transparency under strained states. a) Schematics of typical vertical contraction and image distortions of the stretchable display under strained states and image distortion-free stretchable display with zero Poisson's ratio. b) Typical elastomer with Poisson's ratio of 0.5 (severe vertical contraction, left), and aligned fiber composite for controlling Poisson's ratio near 0 due to the high stiffness of fibers resisting vertical contraction under strained states (right). c) A schematic image of the shear-rolling process of a relatively thick SIBS BCP film for the unidirectional alignment of polystyrene nanocylinders in the elastomer matrix.

the longitudinal direction as $\nu = - \epsilon_t / \epsilon_l$.[9] In particular, easily deformable elastomers used as stretchable substrates suffer from severe vertical contraction with a very high Poisson's ratio of 0.5.[9] To control this material's intrinsic property, new structural approaches to reduce the Poisson's ratio of stretchable substrates are needed.

The auxetic structure, also called a mechanical metamaterial, which has regular inwardly protruding reentrant frameworks, is a good example for enabling a negative Poisson's ratio that expands in the vertical direction when stretched,[10] thus various application research is being conducted in fields such as tissue engineering,[11] actuators,[12] and even stretchable supercapacitors[13] and stretchable lithium-ion batteries.[14] Poisson's ratio can also be controlled using a prestrained wrinkle structure or mechanically anisotropic material. However, among the studies on controlling Poisson's ratio using structural mechanics, little research is related to the distortion in the substrate of display devices requiring transparent characteristics. Only recently, an electroluminescent device with biaxial microwrinkle structure,[15] a kirigami-based auxetic structure microLED system,[16] mechanical metamaterial structure,[17] auxetic-patterned composites[18] and anisotropic composites[19] have been studied. However, these reinforced structures, typically on the millimeter scale, are visibly identifiable and introduce issues such as refraction within the material due to refractive index mismatches between heterogeneous substances. These mismatches

alter the light path, causing reflections at interfaces that lead to glare and a reduction in transparency, with transparency loss proportional to the degree of mismatch. Additionally, the topographically undulated surface of auxetic structures causes undesirable light scattering. During stretching, the significant difference in mechanical properties between the two materials can lead to surface undulations and a nonuniform strain distribution, which are difficult to mitigate.

To address this, an old but novel method for controlling the architectures of the polymer material itself[20,21] can be helpful. Appropriately arranged nanostructures smaller than the wavelength of visible light, such as block copolymers (BCPs), can be considered to control the Poisson's ratio through structural methods while maintaining transparency. The BCPs, in which covalent bonds bind two different polymer chains, form sub-visible wavelength periodic nanostructures through microphase-separation and are a representative material that exhibits thermoplastic elastomer (TPE) properties through the nanostructures.[22] Additionally, in the case of cylindrical BCPs, if the cylinders are aligned in one direction, theoretically in macroscopic composites, there may be a dramatic difference in the modulus between the alignment direction and perpendicular direction, resulting in mechanical anisotropy.[23] Suppose this nanoscopic alignment can effectively prevent macroscopic vertical contraction during stretching. In that case, Poisson's ratio can be easily controlled close to zero and realize a distortion-free transparent,

stretchable substrate, as shown in Figure 1a on the right. Orientation of BCPs can be achieved on chemical[24–27] or topographical patterns[28–30] or through shear alignment[31–33] including our shear-rolling process,[34–37] but has focused only on nanoscale thin films on silicon wafers to enable sub-10 nm patterns in next-generation lithography. Rather, the orientation in relatively thick bulk films[38–40] has been studied only a very long time ago, and little research has been conducted to control the mechanical properties of macroscopic stretchable substrates.[41,42]

In this paper, the shear-rolling process was performed for aligning nano-cylinders of 0.7-mm-thick films of polystyrene-*block*-polyisobutylene-*block*-polystyrene (SIBS) BCP, well known as a typical TPE polymer and having the best gas barrier properties among elastomers,[43] at high temperature in a short time at different roller/substrate speeds. The alignment of the nanocylinders in 0.5 mm thick films also increased as the temperature rose to 200 °C, showing a very high degree of alignment throughout the film, not just in parts. In addition, depending on the degree of alignment of the nanostructure, anisotropy in macroscopic mechanical properties could be induced between the parallel and perpendicular directions of orientation up to 5 times. When the shear-rolled films at different temperatures were used as a transparent and stretchable substrate, the Poisson's ratio can be lowered to a minimum of 0.07. This stretchable substrate with a near-zero Poisson's ratio allows vertical distortion-free, linear pixel displacement, monotonic stress distribution and high transparency without any structural irregularities.

Figure 1b illustrates the stretching configuration of the typical elastomer (left) and the aligned fiber-reinforced composite (right). Due to the low modulus of the elastomer, they can be stretched with a low load, but at the same time, they cannot withstand vertical contraction to conserve their volume while stretching, resulting in a Poisson's ratio of 0.5. In aligned fiber composite,[23] the modulus in the parallel (E_{para}) directions can be described by the arithmetic mean, $E_{para} = E_m V_m + E_f V_f$ and perpendicular (E_{perp}) directions can be expected by harmonic mean, $E_{perp} = \frac{E_m E_f}{E_m V_f + E_f V_m}$, where E and V represent the elastic modulus and volume fraction, and the subscripts m and f represent the matrix and fiber phases (Figure S1, Supporting Information). A large elastic modulus anisotropy along the direction can be predicted when the elastic moduli of the two materials show a large difference and sufficient volume fractions. It is generally known that Poisson's ratio is inversely related to the modulus ratio in a transversely anisotropic material (See the Supporting Information for the detailed information about the correlation between Poisson's ratio and the modulus).[44] Also, as can be seen in the right image of Figure 1b, when aligned cylinders with high modulus resist the vertical contraction force due to tension, the vertical deformation (strain) can be minimized. Therefore, when E_{para} is much bigger than E_{perp}, Poisson's ratio can be reduced to ≈0.

To develop the zero Poisson's ratio film in single materials, we align sub-visible wavelength periodic nanocylinders in the BCP elastomer film using our shear-rolling process. Figure 1c schematically illustrates the unidirectional alignment of the BCP nanostructures through the shear-rolling process.[34] The velocity difference between the roller and the stage applies shear stress (τ) sequentially and momentarily during shear-rolling, so that the

difference in elastic moduli between the relatively stiff nanocylinders and the soft matrix aligns the cylinder structures in the shear direction to become the most energetically stable configuration in the shear environment. The unidirectionally aligned nano-sized cylindrical BCP film produced via the shear-rolling simultaneously exhibits macroscopic mechanical anisotropy similar to fiber alignment and the unity of mechanical and optical properties even under deformation.

To verify whether SIBS BCP can be aligned through shear-rolling in sub-micron thin film geometry as in previous research to align BCP thin films, we first applied this shear-rolling process to 140 nm-thick SIBS films on Si wafers while varying temperature from 140 °C to 220 °C. For the shear-rolling process on the thin films, a 0.8 mm PDMS buffer pad was used to provide good contact and uniform shear stress, and the stage and roller speeds were set to 19 and 20 mm s⁻¹, respectively, to maintain a shear rate (γ) of 1.6 s⁻¹. The process temperatures were set considerably higher than the glass transition temperature of the rigid polystyrene domain (≈100 °C), to allow sufficient mobility of the BCP chains. SEM images and Herman's orientation order parameters[36,45,46] are shown in **Figure 2** (See Figure S2, Supporting Information, for the detailed information about the Herman's orientation parameter). The unsheared film annealed at 200 °C for 12 h showed randomly oriented fingerprint patterns as expected (Figure 2a), and the shear-rolled film at 140 °C showed poorly aligned nanocylinders with a low orientation parameter of 0.12 (Figure 2b). However, directional alignment started to be observed at 160 °C (Figure 2c, their orientation parameter was ≈ 0.68), and the highest directional alignment was observed at 180 °C, which yielded high orientation parameter over 0.93 (Figure 2d). Directional alignments were still observed at 200 °C and 220 °C, with a relatively high degree of orientation parameters of 0.84 and 0.88, as shown in Figure 2e,f, although partial macroscopic peeling of the film was observed. Higher temperatures generally enhance the alignment due to increased polymer mobility. However, elevated temperatures also destabilize the interfaces, leading to macroscopic delamination (Figure S3, Supporting Information) during the shear-rolling process, which resulted in a slight decrease in alignment at 200 °C and 220 °C. This microscopic analysis confirmed that the nanostructure of commercial triblock copolymer-based thermoplastic elastomers could also be successfully oriented by high-temperature shear-rolling.

Next, we performed shear-rolling on a thick bulk SIBS film that can be used as a practical stretchable substrate to investigate whether the unidirectional orientation can be realized throughout the film thickness. First, to confirm whether shear can be applied uniformly throughout the film during shear-rolling, we observed the side of the bulk SIBS film during shear-rolling, as shown in **Figure 3**a–c. When the speeds of the roller and the substrate were the same (Figure 3a), the instantaneous displacements at the top and bottom regions were the same, indicating that no shear was applied. In contrast, when the speeds were different (Figure 3b,c), the instantaneous displacements of the SIBS film formed a constant slope depending on the thickness of the film, confirming that the same shear rate was applied to the entire thick film during the shear-rolling process. However, when the shear rate was high, the difference between the upper and

**ADVANCED
SCIENCE NEWS**

www.advancedsciencenews.com

**ADVANCED
MATERIALS**

www.advmat.de
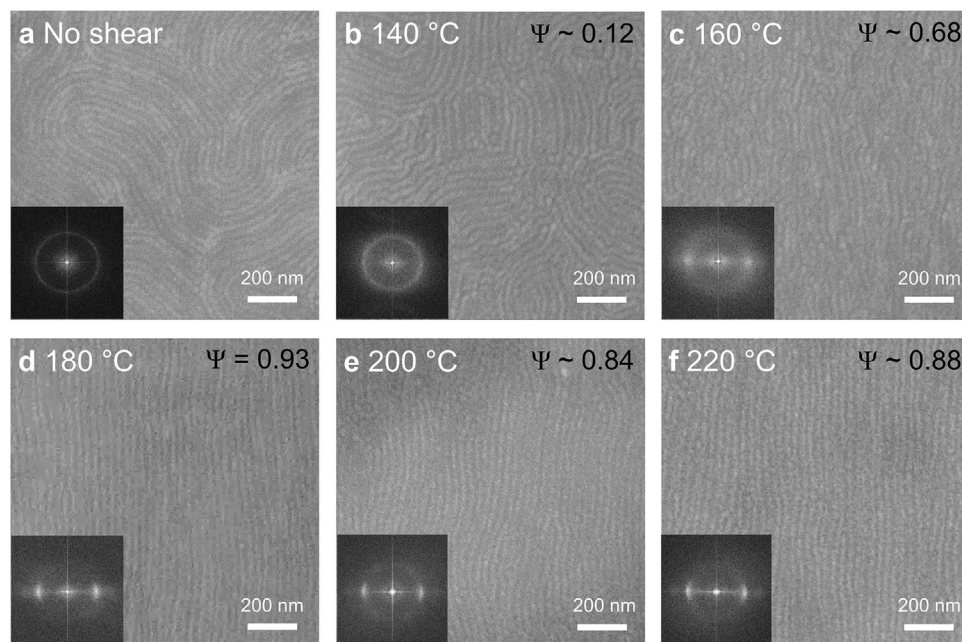
Figure 2. Nanocylinder alignments of 140 nm thick SIBS thin films by shear-rolling process at various temperatures. SEM images of a) pristine SIBS thin film annealed at 200 °C for 12 h, and shear-rolled SIBS thin films at b) 140 °C, c) 160 °C, d) 180 °C, e) 200 °C and f) 220 °C with their fast Fourier transform images and Herman's orientation parameters.
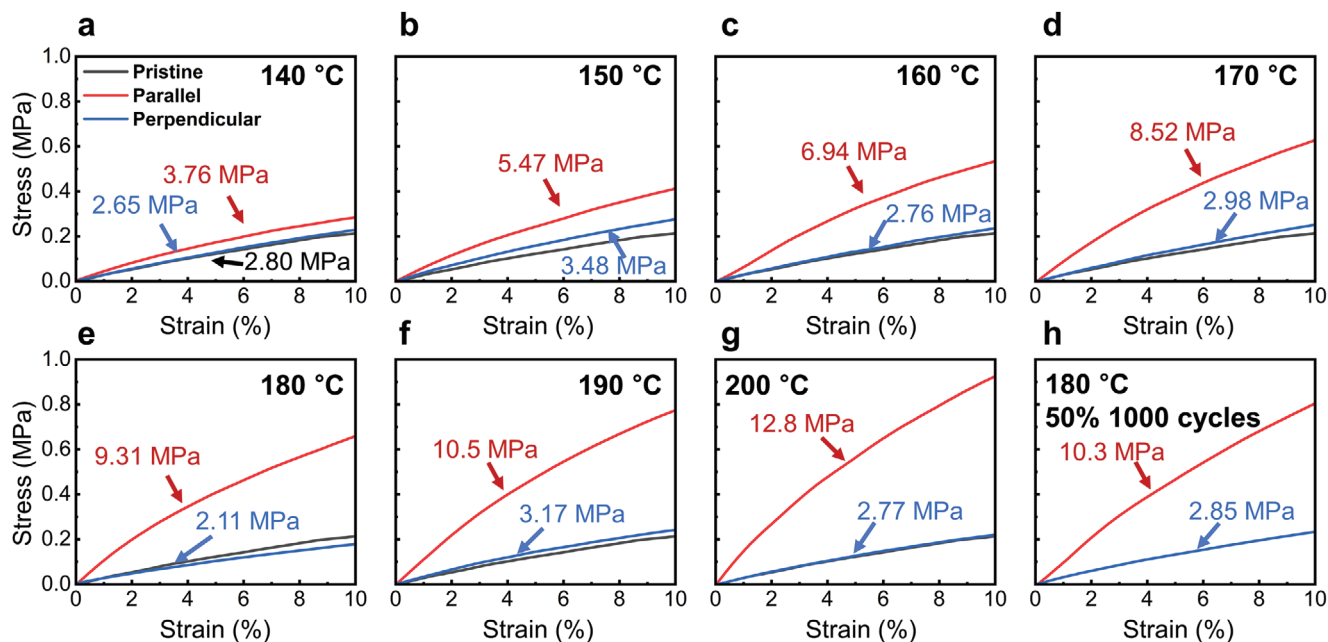
lower strains was large, forming a significant undulating structure on the surface of the film.

Shear-rolling, which had verified that a uniform shear was applied to the bulk film, was executed on 0.7 mm thick transparent SIBS films without a PDMS buffer pad at 180 °C and 20/19 mm s^{-1} to achieve decent alignment while minimizing plastic deformation of the film. To analyze the overall nanostructure ori-

entation of the shear-rolled BCP thick film, transmission-SAXS (TR-SAXS) experiments were performed in three different incident directions: XY-plane, YZ-plane, and XZ-plane, as shown in Figure 3d. As indicated in the schematic, the shear was applied in the X direction. When we obtained SAXS profiles of a unsheared and thermal annealed SIBS film at 180 °C in the XY-plane (normal to film surface), circular scattering patterns
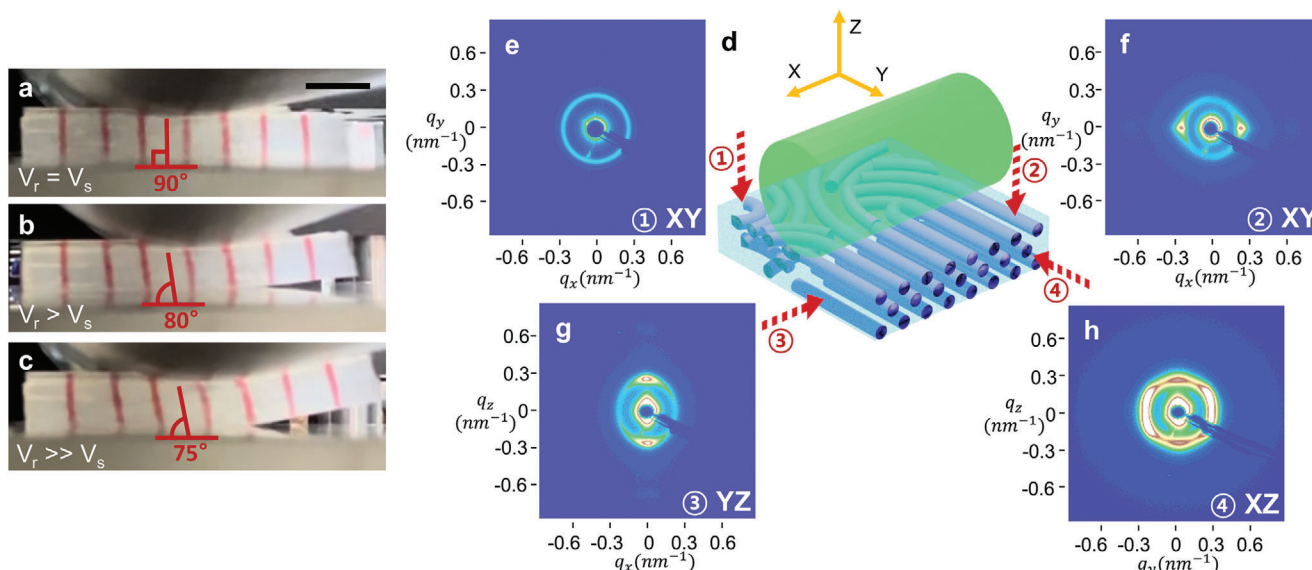
Figure 3. Shear-rolling process to align bulk BCP film and incidence direction-dependent SAXS scattering patterns of shear-rolled BCP films. Side-view photographs of the bulk SIBS films during the rolling process at the same roller speed (V_r) and different stage speed (V_s), a) $V_r = V_s$, b) $V_r > V_s$, c) $V_r \gg V_s$. d) A Schematic diagram of X-ray beam direction to the SIBS thick films in SAXS measurements. SAXS scattering profiles of e) pristine SIBS thick film in XY-plane and shear-rolled SIBS thick films at 180 °C in f) XY, g) YZ, and h) XZ planes.

**ADVANCED
SCIENCE NEWS**

www.advancedsciencenews.com

**ADVANCED
MATERIALS**

www.advmat.de

Figure 4. UTM tensile tests to evaluate the mechanical anisotropy of the shear-rolled SIBS films. Stress-strain curve of the pristine and shear-rolled SIBS films in the alignment and the perpendicular direction and their Young's modulus at different shear-rolling temperatures at a) 140 °C, b) 150 °C, c) 160 °C, d) 170 °C, e) 180 °C, f) 190 °C, g) 200 °C. h) Stress–strain curves of shear-rolled SIBS films at 180 °C after 1000 cycles of stretching/releasing at 50% strain.

indicating randomly oriented periodic nanostructures were observed (Figure 3e). On the other hand, when the shear-rolled film was examined in the same XY-plane (Figure 3f), clear scattering peaks were observed on both sides of the horizontal plane at a q value of 0.023 nm^{-1} (d spacing $\approx$ 26 nm), and higher-order peaks were also observed at 0.044 nm^{-1} and 0.066 nm^{-1}, respectively, confirming the high degree of overall unidirectional alignment of periodic ($\approx$26 nm) nanostructures in the bulk film. When the film was sliced and X-rayed in the YZ-plane (Figure 3g), two vertical peaks with symmetrical top and bottom at a q-value of 0.024 nm^{-1}, and their higher-order peaks were observed, which confirmed that the nanostructures were aligned overall parallel to the shear-rolling direction and periodic in the thickness direction when viewed from the side of the film. The XZ-plane (normal to the shear direction, Figure 3h) showed hexagonal peaks near $q \approx 0.025$ nm^{-1}, indicating highly aligned hexagonally packed nanocylinders and six peaks were identified at 25°, 90°, 155°, 205°, and 270° from the q_x-axis in the azimuthal profile at q values. This pattern indicates that the hexagonally packed nanocylinders are highly aligned parallel to the film, and that this hexagonally packed cylinder structure is slightly elongated in the thickness (z-axis) direction due to the shear force.

In order to investigate whether these nanostructure orientations of thermoplastic elastomers can exhibit macroscopic mechanical anisotropy, tensile tests were performed in directions parallel and perpendicular to the alignment using a universal tensile machine (UTM). Stress–strain curves of pristine SIBS film and shear-rolled films at different temperatures in the alignment and perpendicular directions were obtained, and Young's moduli for the initial strain were extracted through the slopes because the films undergo compression in the orientation direction during

stretching, as shown in **Figure 4**. While the modulus in the direction perpendicular to the alignment did not change much at around 2.8 MPa with increasing shear-rolling temperature, the moduli in the alignment direction increased significantly from 3.8 MPa to 5.5, 6.9, 8.5, 9.3, 10.5, and 12.8 MPa with increasing shear-rolling temperature from 140 °C to 200 °C. Just as the degree of orientation of the thin films increased with increasing shear temperature in Figure 2, shear-rolled SIBS thick films with increasing temperature also exhibited increased mechanical anisotropy and widely controlled anisotropy ratios of 1.42, 1.57, 2.51, 2.86, 4.41, 3.31 and 4.62 times, respectively. The whole stress-strain curve of the 180 °C shear-rolled SIBS film in alignment and perpendicular directions and the pristine SIBS until the fracture is shown in Figure S4 in Supporting Information. These anisotropies are due to the polystyrene nanocylinders of high modulus ($\approx$3 GPa) being oriented in one direction in the polyisobutylene matrix of low modulus ($\approx$0.8 MPa) and explained by the difference in modulus in the orientation direction and the direction perpendicular in the continuous and aligned fiber composites.[23] This mechanical anisotropy in shear-rolled SIBS films can be maintained without losing anisotropy even after repeated 50% stretching over 1000 times, as shown in Figure 4h.

We then investigated whether the Poisson's ratio can actually be reduced to close to zero when the films with aligned nanostructures and mechanical anisotropy are stretched in one direction. The photographs comparing the vertical distortion between the pristine SIBS film and the 180 °C shear-rolled SIBS films under uniaxial strains at 50% are shown in **Figure 5a–c** and various deformations in Figure S5 (Supporting Information). While the pristine SIBS film showed significantly curved edges (red line) due to the vertical contraction commonly seen
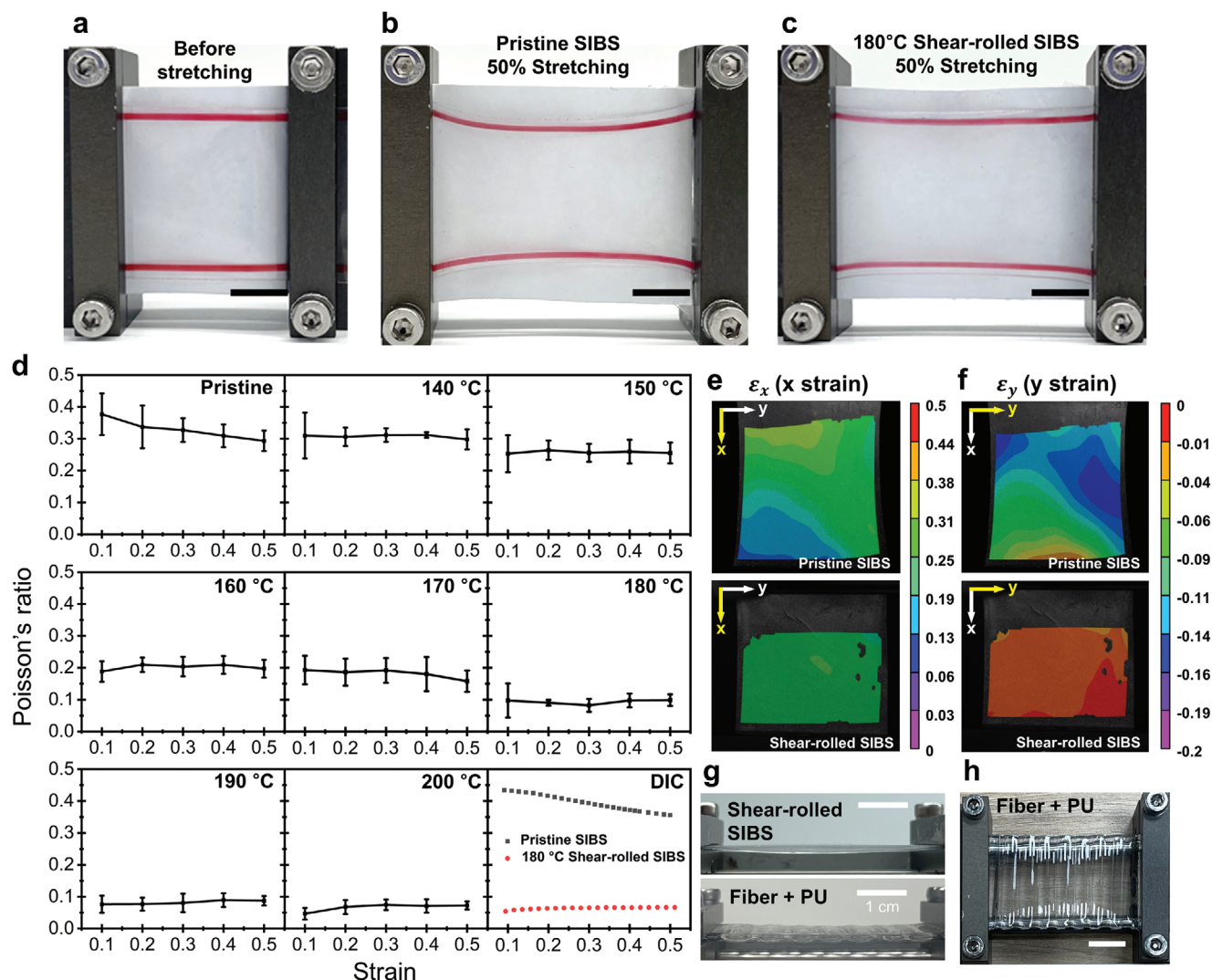
Figure 5. Vertical contraction/distortion difference between the pristine and the shear-rolled SIBS films during stretching, x and y-directions strain distribution and Poisson's ratio of the pristine and shear-rolled SIBS films during stretching. Photographic images of a) unstrained SIBS film, b) the pristine SIBS film under 50% strain, and c) 180 °C shear-rolled SIBS film under 50% strain. d) The variation in Poisson's ratios extracted from photographic images and DIC measurements of the pristine and shear-rolled SIBS films at different process temperatures from 140 °C to 200 °C. e,f) Measured strain distributions of the pristine and the 180 °C shear-rolled SIBS film at 30% stretching using DIC e) in tensile (x) direction and f) in vertical (y) direction. g) The height variation in the thickness (z-axis) direction at the strained state of our shear-rolled SIBS film and structurally reinforced polyurethane composite film with millimeter-sized aligned fibers and h) the resulting top-view reflection of light and visually noticeable image.

in elastomers when stretched by 50% (Figure 5b), the shear-rolled SIBS film maintained a low curvature and straight edges like an elongated rectangle without vertical deformation even after 50% stretching (Figure 5c). This reveals that the nanostructure alignment can indeed effectively prevent vertical contraction and image distortion of stretchable substrate. In addition, the shear-rolled SIBS film maintained high transparency (84.9%) without any visual difference before and after orientation because the nanostructures were aligned smaller than the visible light and the transparency did not decrease (84.5%) even when stretched (Figure S6, Supporting Information). This demonstrates that mechanical anisotropy can be implemented without any decrease in optical properties by nanostructure orientation, and a fully transparent stretchable substrate with

effective vertical shrinkage and no image distortion can be realized.

The values of Poisson's ratios were measured by image analysis for the shear-rolled films at various temperatures at strains ranging from 10% to 50% (Figure 5d). Overall, the Poisson's ratios did not vary significantly with strains, and the pristine SIBS films and the shear-rolled films at 140 °C exhibited relatively high Poisson's ratios of 0.3–0.4 up to 50% strain. However, at 150 °C, the Poisson's ratio was reduced to 0.26 and gradually decreased as the processing temperature increased, showing a ratio of 0.20 and 0.18 at 160 °C and 170 °C, respectively. Finally, the Poisson's ratios of higher temperatures were close to zero, reaching 0.08 at 180 °C and 0.07 at 190 and 200 °C. As explained above, as the shear-rolling temperature increases, the degree of

orientation of the nanostructure increases, which makes the mechanical anisotropy more prominent, and accordingly, the Poisson's ratio ultimately can be controlled as desired from the typical value of 0.4 to close to 0. In addition, the Poisson's ratio in bulk films can continue to decrease up to 200 °C, unlike thin films, due to the reduced effects of surface and interfaces and the heat transfer into the thick film. We also confirmed that the Poisson's ratios of the 180 °C shear-rolled SIBS maintained low values less than 0.08 up to 100% strain (Figure S7, Supporting Information), and the preservation of aligned nanocylinder structure without breakage was confirmed by performing TR-SAXS measurements under stretching conditions up to 100% (Figure S8, Supporting Information). For more precise measurement, we measured the Poisson's ratio using digital image correlation (DIC) measurements of the 180 °C shear-rolled SIBS film for both the horizontal and vertical full centerlines. While the Poisson's ratios of the pristine film gradually decreased but still maintained high values from 0.5 to 0.35 under strained states up to 50%, the 180 °C shear-rolled film maintained a consistent and much lower Poisson's ratio of ≈0.068 in wide ranges of strains up to 50%. Moreover, to generalize the shear-rolling approach, another commercial cylindrical SBS thermoplastic elastomer was tested (Figure S11, Supporting Information). The pristine SBS flim exhibited a Poisson's ratio of 0.35–0.40, whereas the 300 °C shear-rolled SBS film exhibited a lower Poisson's ratio in the range of 0.15–0.22. This suggests the potential for controlling Poisson's ratio in general BCP elastomer films through our shear-rolling process.

To verify that the deformation occurs uniformly at all points of the shear-rolled films, the actual x-axis (strain direction) and y-axis (normal to strain) direction strain distributions at every single point of the pristine and shear-rolled SIBS films were investigated using digital image correlation (DIC) measurements at 30% strain in Figure 5e,f and Video S1 (Supporting Information). The pristine SIBS film showed a larger elongation in the tensile (x-axis) direction and larger contraction in the y-axis at the center of the film than around the jig at the edges of the film, and large strain variations in the overall x- and y-axis because the jig holding the film prevents vertical contraction at the edge (additional DIC measurements in Figure S9, Supporting Information). However, our aligned nanostructured films exhibited a consistently uniform and monotonic strain distribution in both the tensile (x) and vertical (y) directions during tensile loading, especially near-zero strain in the vertical direction over the entire area. Even in the thickness direction, the shear-rolled film maintained a monotonic and flat shape without any height undulation under stretching (Figure 5g). These results indicate very uniform x-, y-, and z-direction deformations in every microscopic part of the entire area under tension, which can be an excellent approach to minimize image distortion in stretchable substrates. Previous studies[15–19] have shown that controlling the Poisson's ratio through micron-scale structural approaches (e.g., wrinkles, auxetic reentrant) generates differently deformed microstructures with different elastic moduli in the matrix under mechanical strain, which can be observed as surface topographical undulations, microscopic strain variation, and optically revealed structures, as shown in Figure 5g. In particular, these regularly aligned nanostructures with a period of less than 30 nm, which is much smaller than the wavelength of visible light, possess mechanical anisotropy while also possessing one-body me-

chanical deformation and optical properties, which simultaneously ensure monotonous and consistent transparency and uniform mechanical deformation in the x-, y-, and z-directions without any distortion even in microscopic parts, and thus can be a promising candidate as an ideal substrate for stretchable displays.

To investigate the prevention of image distortion through control of Poisson's ratio, we demonstrated a stretchable LED device and a stretchable printed image on the SIBS substrate (**Figure 6**a–e). As shown in Figure 6a, mini-LEDs were attached onto the SIBS film, forming a grid with a spacing of 3 mm, and interconnected via liquid metal printing. After 50% stretching, the lit mini-LED grid on the pristine SIBS film exhibited significant vertical contraction between LEDs, with some LEDs rotating by up to 20° (Figure 6b and Figure S10b, Supporting Information). In contrast, the lit mini-LED grid on the shear-rolled SIBS film showed minimal changes in vertical distance and only slight rotation of less than 5° even after 50% stretching (Figure 6c and Figure S10c, Supporting Information). Quantitatively, the Poisson's ratio calculated from the distance changes between two centrally located LEDs was 0.44 for the pristine SIBS film and 0.09 for the shear-rolled SIBS film. Finally, we printed a pixelated image onto the SIBS substrate (Figure 6d–f). Upon stretching the pristine SIBS substrate by 50%, each pixel contracted contracted in the vertical direction and rotated due to the high Poisson's ratio, resulting in the distortion of the image into curved shapes (Figure 6e). In contrast, when the shear-rolled SIBS substrate was stretched by 50%, the square pixels exhibited minimal vertical shrinkage and distortion, preserving the clarity of the image (Figure 6f). This demonstration proves how a high Poisson's ratio leads to image distortion upon stretching and that controlling the Poisson's ratio can effectively preserve image clarity.

2. Conclusion

In summary, this study presents a pioneering approach to address a critical challenge in stretchable device technology—achieving a fully transparent and monotonically stretchable substrate with controlled Poisson's ratio to minimize undesirable vertical deformation during stretching. By utilizing a shear-rolling process on 0.7 mm thick films of SIBS BCPs, renowned for their TPE properties and exceptional gas barrier characteristics, we successfully aligned nanocylinders within the SIBS film, showcasing high degrees of orientation, particularly at elevated temperatures. This alignment correlated with increased mechanical anisotropy, resulting in up to a fivefold difference in modulus between the aligned and perpendicular directions, maintained even after extensive stretching. Importantly, our methodology allowed precise control of the Poisson's ratio, reducing it from 0.32 at 140 °C to near-zero values at 200 °C. The shear-rolled BCP films exhibited consistent and monotonic strain distribution, ensuring minimal vertical deformation and distortion, particularly under 50% strain, making them promising candidates for distortion-free stretchable displays. In particular, since we demonstrate that mechanical deformation can be controlled by universally orienting nanostructures using general BCPs, this research sets the stage for the development of transparent and stretchable devices with controlled mechanical performance. Future work could explore broader applications, including wearable electronics, stretchable or deformable displays, and soft robotics,

ADVANCED
SCIENCE NEWS

www.advancedsciencenews.com

ADVANCED
MATERIALS

www.advmat.de
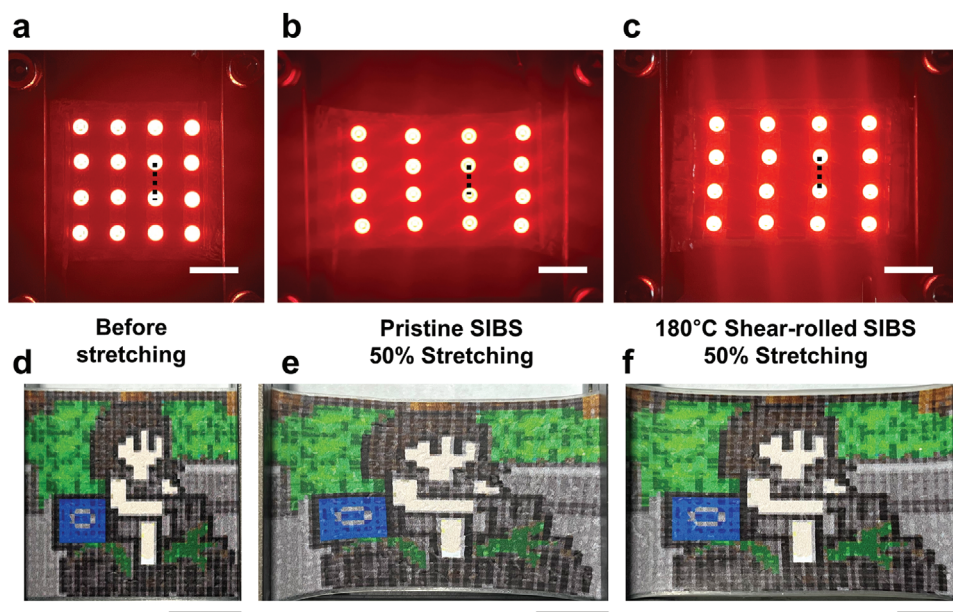
Figure 6. Visualization of vertical distortion and deformation differences between pristine and shear-rolled SIBS films using a mini-LED device and printed images on SIBS substrates. Photographs of a) the unstretched device and d) the printed image; b) the device and e) the printed image on a pristine SIBS substrate stretched by 50%. c) the device and f) the printed image on a shear-rolled SIBS substrate stretched by 50%. The white scale bars in (a–c) and the black scale bars in (d–f) each represent 1 cm.

leveraging the unique mechanical and optical properties of shear-rolled substrates to advance the field of stretchable electronics. Additionally, further investigations into scalability and integration with various device architectures will be crucial for the practical realization of these advancements.

3. Experimental Section

Materials and Sample Preparation: Polystyrene-*b*-polyisobutylene-*b*-polystyrene), PS-*b*-PIB-*b*-PS (SIBS, 9-42-9 kg mol^{-1}), especially SIBSTAR 73T was provided by Kaneka Co, Japan. Polystyrene-*b*-polybutadiene-*b*-polystyrene (SBS) KTR401 was obtained from Kumho Petrochemical. A SIBS in toluene solution (10 wt%) was centrifuged at 7000 rpm for 20 min to remove impurities. Purified SIBS in toluene solution (3 wt%) was spin-coated at 2000 rpm for 30 s onto ultraviolet ozone (UVO) (AC-6; AhTech LTS) treated (30 min) Si wafer, forming 140 nm thin films. The spin-coated thin films were thermally annealed at 200 °C under a vacuum for 12 h. The polydimethylsiloxane (PDMS; Sylgard 184 from Dow Corning) buffer pads were prepared by mixing prepolymer and curing agent in a 5:1 ratio and poured in a 1 mm thick mold on a Si wafer. The poured PDMS was cured at 60 °C for 12 h and then at 180 °C for 3 h. To produce 0.7 mm thickness SIBS films, the SIBSTAR 73T pellet was hot pressed at 210 °C, 1.5 tons for 10 min with 5 cm × 5 cm or 13 cm × 13 cm square, 0.5 mm thickness stainless square mold. To fabricate the fiber–polyurethane (PU) composite (ClearFlex 30, Smooth-On, Inc.), 20 μm thick polypropylene films (Youl-Chon Chemical Co., Ltd.) were cut to 3 mm width ribbons and aligned inside a 2 mm silicone mold. The PU prepolymer and cross-linking agents were mixed at a 1:1 ratio and then poured into the mold containing the aligned polypropylene ribbons. The assembly was cured at 80 °C for 2 h. After curing, the ribbon–PU composite was stretched up to 50% strain using a custom-built stretching machine.

Shear-Rolling Process: Prior to the process, the stage was preheated at the desired temperatures for 10 min to maintain a constant temperature. Both during the SIBS thin film shear-rolling and SIBS thick film shear-rolling, the speed of the stage and the roller were fixed at 19 and 20 mm

s^{-1}, respectively. A PDMS pad was attached to the roller for the thin film process, while 0.065 mm polyimide tape was attached to the roller for the thick film process. SIBS thin films on the Si wafer were preannealed for 5 s at the stage to establish the thermal equilibrium for all temperatures. Free-standing SIBS thick films were also processed onto the Si wafer, preannealed 15 s for 140–180 °C and 5 s for 190 °C and 200 °C to avoid tearing or damage.

Characterization: The SEM images of the shear-rolled SIBS film were obtained using field-emission scanning electron microscopy (FE-SEM, Zeiss Sigma 300, Zeiss). For intensifying contrast between the polystyrene phase and the polyisobutylene phase, the SIBS thin films were treated with oxygen plasma (Vita, Femto Science Inc., 20 sccm, 20 mTorr) at 200 W for 10 s before the measurements. Fast Fourier transform (FFT) analysis processed from 30 000× magnification SEM images using the ImageJ program. Grazing incidence small-angle X-ray scattering (GISAXS) and transmission small-angle X-ray scattering (TrSAXS) were performed at the 9A beamline of the Pohang Light Source. The wavelength of the X-ray was 1.1190 Å (11.08 keV), and the sample to detector distances were 2543.3 mm and 2556.8 mm for GISAXS and TrSAXS, respectively. Tensile tests were executed using universal testing machine (UTM; INSTRON model 5966). Specimens of the tensile test were prepared in accordance with ISO 37 type 3 (overall length 50 mm, length and the width of the narrow portion 16 mm, 4 mm respectively) and the specimen were stretched at a rate of 5 mm min^{-1}. The specimens for measuring the Poisson's ratio were prepared in a 5 cm × 3 cm rectangular shape, and specimens were stretched at 10%, 20%, 30%, 40%, and 50% by lab-made stretching equipment. After stretching, digital images of the specimen were acquired, and the lengths of the lines from multiple points were measured using the ImageJ program. The specimens of the DIC measurements were prepared in 4.3 cm × 7 cm rectangular shape. For obtaining Poisson's ratio, *x*- and *y*-axis strains were measured on the whole center lines of the film, obtained by using DIC software and VIC-2D (correlated SOLUTIONS). A Shear-rolled SIBS film was repetitively stretched 0% to 30% strain 1000 times, at a rate of 1000% per minute, using the lab-made automatic stretching machine. To measure the transmittance of the films, an ultraviolet-visible-near-infrared spectrometer (V-600, Jasco) was used with lab-made stretching equipment.

Fabrication of Stretchable Mini-LED Device and Printing Image on SIBS Films: To demonstrate the stretchable mini-LED device, we first patterned an EGaIn (eutectic gallium–indium alloy) circuit using a polyimide film cut by a laser cutter as a stencil. The polyimide stencil was placed on the SIBS substrate, and EGaIn was deposited to form the desired circuit pattern. Mini-LEDs (dimensions: 2.8 mm × 3.5 mm × 1.9 mm; model ASMM-CR03-AS402, Broadcom) were then attached to the designated positions on the SIBS substrate using double-sided tape. Electrical power was supplied to the device using a power supply (U3401A, Keysight Technologies). The device was stretched using a custom-built stretching machine to observe the mechanical and electrical performance under strain. To create the stretchable printed image on the SIBS substrate, we utilized a copyright-approved image. The image was printed onto the SIBS substrate using polyurethane ink in a process carried out by SNSPrintTec. The printed substrates were then stretched using a custom-built stretching machine.

Supporting Information

Supporting Information is available from the Wiley Online Library or from the author.

Acknowledgements

Conflict of Interest

The authors declare no conflict of interest.

Data Availability Statement

The data that support the findings of this study are available from the corresponding author upon reasonable request.

Keywords

[1] N. Matsuhisa, S. Niu, S. J. K. O'Neill, J. Kang, Y. Ochiai, T. Katsumata, H.-C. Wu, M. Ashizawa, G.-J. N. Wang, D. Zhong, X. Wang, X. Gong, R. Ning, H. Gong, I. You, Y. Zheng, Z. Zhang, J. B.-H. Tok, X. Chen, Z. Bao, *Nature* **2021**, *600*, 246.

[2] N. Matsuhisa, D. Inoue, P. Zalar, H. Jin, Y. Matsuba, A. Itoh, T. Yokota, D. Hashizume, T. Someya, *Nat. Mater.* **2017**, *16*, 834.

[3] J. Guo, B. Zhou, C. Yang, Q. Dai, L. Kong, *Adv. Funct. Mater.* **2019**, *29*, 1902898.

[4] S. Zhang, A. Chhetry, M. A. Zahed, S. Sharma, C. Park, S. Yoon, J. Y. Park, *npj Flexible Electron.* **2022**, *6*, 11.

[5] Y. Liu, M. Pharr, G. A. Salvatore, *ACS Nano* **2017**, *11*, 9614.

[6] J. C. Yeo, H. K. Yap, W. Xi, Z. Wang, C. Yeow, C. T. Lim, *Adv. Mater. Technol.* **2016**, *1*, 1600018.

[7] W. Wu, W. C. Poh, J. Lv, S. Chen, D. Gao, F. Yu, H. Wang, H. Fang, H. Wang, P. S. Lee, *Adv. Energy Mater.* **2023**, *13*, 2204103.

[8] M. S. Kim, Y. Lee, J. Ahn, S. Kim, K. Kang, H. Lim, B. Bae, I. Park, *Adv. Funct. Mater.* **2023**, *33*, 2208792.

[9] G. N. Greaves, A. L. Greer, R. S. Lakes, T. Rouxel, *Nat. Mater.* **2011**, *10*, 823.

[10] K. E. Evans, A. Alderson, *Adv. Mater.* **2000**, *12*, 617.

[11] W. Zhang, P. Soman, K. Meggs, X. Qu, S. Chen, *Adv. Funct. Mater.* **2013**, *23*, 3226.

[12] A. Lazarus, P. M. Reis, *Adv. Eng. Mater.* **2015**, *17*, 815.

[13] B. S. Kim, K. Lee, S. Kang, S. Lee, J. B. Pyo, I. S. Choi, K. Char, J. H. Park, S. S. Lee, J. Lee, J. G. Son, *Nanoscale* **2017**, *9*, 13272.

[14] S. Kang, S. Y. Hong, N. Kim, J. Oh, M. Park, K. Y. Chung, S.-S. Lee, J. Lee, J. G. Son, *ACS Nano* **2020**, *14*, 3660.

[15] S. Jeong, H. Yoon, B. Lee, S. Lee, Y. Hong, *Adv. Mater. Technol.* **2020**, *5*, 2000231.

[16] B. Jang, S. Won, J. Kim, J. Kim, M. Oh, H. Lee, J. Kim, *Adv. Funct. Mater.* **2022**, *32*, 2113299.

[17] J.-C. Choi, H. Y. Jeong, J.-H. Sun, J. Byun, J. Oh, S. J. Hwang, P. Lee, D. W. Lee, J. G. Son, S. Lee, S. Chung, *Adv. Funct. Mater.* **2024**, 2406725.

[18] Y. Lee, B. Jang, H. Song, S. Kim, Y. W. Kwon, H. S. Kang, M. S. Kim, I. Park, T.-S. Kim, J. Jang, J.-H. Kim, J.-U. Park, B.-S. Bae, *Nat. Commun.* **2024**, *15*, 7146.

[19] H. Oh, J. Hur, S. Jeong, S.-H. Heo, D.-C Lee, Y. Hong, S. Chung, J. Lee, J. G. Son, *Composites, Part A* **2024**, *185*, 108338.

[20] J. Kim, G. Zhang, M. Shi, Z. Suo, *Science* **2021**, *374*, 212.

[21] J. Steck, J. Kim, Y. Kutsovsky, Z. Suo, *Nature* **2023**, *624*, 303.

[22] G. Holden, E. T. Bishop, N. R. Legge, *J. Polym. Sci. Part C: Polym. Symp.* **1969**, *26*, 37.

[23] W. D. Callister Jr., D. G. Rethwisch, (Eds: L. Ratts), *Materials Science and Engineering: An Introduction*, 10th ed., Wiley, New York **2018**, pp. 564–606.

[24] C. -C. Liu, A. Ramírez-Hernández, E. Han, G. S. W. Craig, Y. Tada, H. Yoshida, H. Kang, S. Ji, P. Gopalan, J. J. de Pablo, P. F. Nealey, *Macromolecules* **2013**, *46*, 1415.

[25] R. Ruiz, H. Kang, F. A. Detcheverry, E. Dobisz, D. S. Kercher, T. R. Albrecht, J. J. de Pablo, P. F. Nealey, *Science* **2008**, *321*, 936.

[26] S. O. Kim, H. H. Solak, M. P. Stoykovich, N. J. Ferrier, J. J. de Pablo, P. F. Nealey, *Nature* **2003**, *424*, 411.

[27] C.-C. Liu, E. Franke, Y. Mignot, R. Xie, C. W. Yeung, J. Zhang, C. Chi, C. Zhang, R. Farrell, K. Lai, H. Tsai, N. Felix, D. Corliss, *Nat. Electron.* **2018**, *1*, 562.

[28] I. Bita, J. K. W. Yang, Y. S. Jung, C. A. Ross, E. L. Thomas, K. K. Berggren, *Science* **2008**, *321*, 939.

[29] J. K. W. Yang, Y. S. Jung, J.-B. Chang, R. A. Mickiewicz, A. Alexander-Katz, C. A. Ross, K. K. Berggren, *Nat. Nanotechnol.* **2010**, *5*, 256.

[30] R. A. Segalman, H. Yokoyama, E. J. Kramer, *Adv. Mater.* **2001**, *13*, 1152.

[31] D. E. Angelescu, J. H. Waller, D. H. Adamson, P. Deshpande, S. Y. Chou, R. A. Register, P. M. Chaikin, *Adv. Mater.* **2004**, *16*, 1736.

[32] Y. C. Kim, T. J. Shin, S.-M. Hur, S. J. Kwon, S. Y. Kim, *Sci. Adv.* **2019**, *5*, eaaw3974.

[33] P. W. Majewski, A. Rahman, C. T. Black, K. G. Yager, *Nat. Commun.* **2015**, *6*, 7448.

[34] J. Oh, M. Shin, I. S. Kim, H. S. Suh, Y. Kim, J. K. Kim, J. Bang, B. Yeom, J. G. Son, *ACS Nano* **2021**, *15*, 8549.

[35] J. Cho, M. Hwang, M. Shin, J. Oh, J. Cho, J. G. Son, B. Yeom, *ACS Nano* **2021**, *15*, 17463.

2414794 (9 of 10)

**ADVANCED
SCIENCE NEWS**

www.advancedsciencenews.com

**ADVANCED
MATERIALS**

www.advmat.de

[36] J. Cho, J. Oh, J. Bang, J. H. Koh, H. Y. Jeong, S. Chung, J. G. Son, *Nat. Commun.* **2023**, *14*, 8412.

[37] W. H. Nam, J. Hur, J. Cho, D. Y. Ryu, H. Ahn, J. G. Son, *Small* **2024**, 2405717.

[38] J. Sänger, W. Gronski, H. Leist, U. Wiesner, *Macromolecules* **1997**, *30*, 7621.

[39] C. Osuji, Y. Zhang, G. Mao, C. K. Ober, E. L. Thomas, *Macromolecules* **1999**, *32*, 7703.

[40] R. J. Albalak, E. L. Thomas, *J. Polym. Sci. Part B: Polym. Phys.* **1994**, *32*, 341.

[41] M. J. Folkes, A. Keller, *Polymer* **1971**, *12*, 222.

[42] C. Ye, G. Singh, M. L. Wadley, A. Karim, K. A. Cavicchi, B. D. Vogt, *Macromolecules* **2013**, *46*, 8608.

[43] Y. Shao, J. Yan, Y. Zhi, C. Li, Q. Li, K. Wang, R. Xia, X. Xiang, L. Liu, G. Chen, H. Zhang, D. Cai, H. Wang, X. Cheng, C. Yang, F. Ren, Y. Yu, *Nat. Commun.* **2024**, *15*, 6106.

[44] C. Kohlhauser, C. Hellmich, *Eur. J. Mech. A Solids* **2012**, *33*, 82.

[45] J. J. Hermans, P. H. Hermans, D. Vermaas, A. Weidinger, *Rec. Trav. Chim. Pays-Bas* **1946**, *65*, 427.

[46] A. Kaniyoor, T. S. Gspann, J. E. Mizen, J. A. Elliott, *J. Appl. Polym. Sci.* **2021**, *138*, 50939.